



Power Electronic Systems
Laboratory

© 2011 IEEE

Proceedings of the 8th International Conference on Power Electronics (ECCE Asia 2011), The Shilla Jeju, Korea,
May 30-June 3, 2011.

Multi-Objective Optimization of Ultra-flat Magnetic Components with a PCB-Integrated Core

C. Marxgut
J. Mühlethaler
F. Krismer
J.W. Kolar

This material is posted here with permission of the IEEE. Such permission of the IEEE does not in any way imply IEEE endorsement of any of ETH Zurich's products or services. Internal or personal use of this material is permitted. However, permission to reprint/republish this material for advertising or promotional purposes or for creating new collective works for resale or redistribution must be obtained from the IEEE by writing to pubs-permissions@ieee.org. By choosing to view this document, you agree to all provisions of the copyright laws protecting it.



Eidgenössische Technische Hochschule Zürich
Swiss Federal Institute of Technology Zurich

Multi-Objective Optimization of Ultra-flat Magnetic Components with a PCB-Integrated Core

C. Marxgut, J. Mühlethaler, F. Krismer, and J.W. Kolar
Power Electronic Systems Laboratory, ETH Zurich
Email: marxgut@lem.ee.ethz.ch, www.pes.ee.ethz.ch

Abstract—In future applications, e.g. in ultra-flat OLED lamp drivers or flat screen power supplies, ultra-flat power systems are highly demanded. Therefore, the design and implementation of a PCB-integrated flyback transformer for a 1 mm thin PFC rectifier is under investigation. In this paper, an overview on several integration methods is given. It is shown that the PCB-integration of magnetic cores results in the required thickness of 1 mm and in a high energy density. Therefore, the design and the realization of ultra-flat magnetic components with PCB-integrated cores is detailed in this paper. The presented multi-objective design procedure determines the inductor and/or transformer setup optimal with respect to minimal losses and/or minimal footprint; for this purpose, the proposed design procedure considers all required electrical, magnetical, and geometrical parameters of the magnetic component. Furthermore, the design procedure accounts for anisotropic core loss behavior and includes an accurate reluctance model. Experimental results are used to verify the design procedure.

Index Terms—Ultra-flat Magnetics, PCB-integrated Inductor, PCB-integrated Transformer, Power Sheet

I. INTRODUCTION

Ultra-flat power converters are increasingly needed for specific future applications, as e.g. ultra-flat OLED lamp drivers [1]–[3] or flat screen power supplies [4]. The respective power converters are single-phase power factor correction (PFC) rectifiers, which provide an output power between 20 W and 200 W at a constant dc voltage (typically 10...20 V); the total converter height limit is typically 1...2 cm [5].

The Power Electronic Systems Laboratory at ETH Zurich aims to outperform this height requirement by a factor of 10 and to realize a PFC rectifier with a total height of only 1 mm. The related research project, entitled *The Power Sheet* [6], focuses on the analysis and the comprehension of the implications of the extremely low converter height on the rectifier's efficiency and on the total footprint required for the PFC rectifier. Furthermore, different trade-offs regarding the optimal converter design, with respect to converter efficiency or converter footprint, are investigated.

Except for the magnetic components, all converter components are available either in thin packages with thicknesses of less than 1 mm or as bare chips, i.e. thin SMD packaged semiconductor components (e.g. power MOSFETs, control ICs) and thin ceramic capacitors with thicknesses of less than 1 mm are commercially available [7], [8]. Printed circuit boards (PCB) with a total thickness of less than 1 mm can be realized and the above mentioned components (semiconductors, capacitors, control circuits) can be embedded into the PCB [9]. Thus, the implementation of ultra-flat magnetic

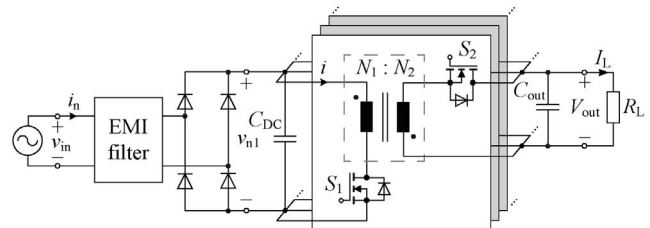


Fig. 1. Flyback-type PFC rectifier system, specified in Table I. The system is split up into several parallel interleaved modules in order to reduce the input and output capacitor currents and to reduce the total footprint of the transformers which are highlighted in the figure.

components is the main challenge that needs to be solved in order to realize the 1 mm thin PFC rectifier.

In an initial step, power SMD inductors could be considered; however, the total height of the flattest available power SMD inductors is over 3 mm [10]. As an alternative, planar magnetic cores and a multilayer PCB could be used to realize ultra-flat magnetic components. Still, the realization of the required ultra-flat magnetic components is unfeasible, since the minimal total height of available planar cores is 5 mm (e.g. ELP 14/3.5/5 by [11]). In a different approach, flat magnetic components could be implemented with PCB air inductors, which are covered with magnetic material. In [12] a transformer based on this integration method is used for a 60 W power converter (PCB thickness: 4 mm). The implemented core employs a ferrite polymer compound with a low permeability (typ. $\mu_r = 10...20$); therefore, a considerable area is required in order to obtain a desired inductance value. This technique facilitates the realization of thin inductors, however, the energy density of these inductors is low due to the large air gap length employed. It is found that the core of the magnetic component needs to be integrated into the PCB in order to reduce the air gap length and to

TABLE I
SPECIFICATIONS OF THE POWER SHEET AT A THICKNESS OF 1 mm AND A FOOTPRINT OF AN A4 PAGE.

Quantity	Value
V_{in}	= 230 V _{rms}
V_{out}	= 20 V
P_{out}	= 200 W
f_s	= 160 kHz...320 kHz
T_{amb}	= 45 °C
Galvanically isolated	

increase the energy density. In [13] the PCB integration of high permeable magnetic materials ($\text{Ni}_{80}\text{Fe}_{20}$) is discussed; PCB-integrated core structures with a thickness of 1.3 mm have been built and are used as inductors in a 1.5 W buck converter. A comparison between closed core structures and air inductors is given and it is shown that closed core assemblies provide the highest inductance and efficiency levels per area. However, due to the thin magnetic core ($10 - 20 \mu\text{m}$), a large area is required to avoid saturation for a given current and to achieve a required inductance value. Furthermore, the eddy current losses in magnetic foils are large due to the spiral winding arrangement. In [14] a ferrite core (Ferroxcube 3F3 [15]) is integrated into a PCB and applied to a buck converter ($3.3 \text{ V}/20 \text{ A}$). The inductance value is $1 \mu\text{H}$ and the integrated core has a thickness of 2 mm. Ferrite materials feature low core losses. However, ferrite is very brittle and as the required magnetic cores are extremely thin ($< 1 \text{ mm}$) the production of ferrite cores is very difficult. Therefore, ferrites are not considered as an appropriate choice. Thus, amorphous and nanocrystalline soft magnetic materials remain, which enable the manufacturing of cores less fragile than ferrite cores. Fig. 2 illustrates the construction of a magnetic component with PCB-integrated core.

This paper investigates the applicability of nanocrystalline and amorphous soft magnetic materials for the realization of ultra-flat magnetic components. This is illustrated on the example of the high frequency (HF) transformer of a single-phase flyback-type PFC rectifier with a total converter height of 1 mm and specifications according to Table I. The considered PFC rectifier as presented in Fig. 1 employs synchronous rectification and operates with zero voltage switching (ZVS), close to the boundary between continuous conduction mode (CCM) and discontinuous conduction mode (DCM), to achieve low switching losses [16]. The flyback-type PFC rectifier employs only a single magnetic power component, i.e. the flyback transformer. A more common approach with input-side boost-type PFC rectifier and series connected dc-dc converter shows a larger footprint than the flyback-type PFC rectifier, due to the two required magnetic components, i.e. the boost inductor and the HF transformer of the dc-dc converter.

Section II summarizes the properties of the considered magnetic materials and discusses stacked and toroidal wound core constructions of PCB-integrated magnetic components. Special focus will be laid on the anisotropy of the magnetic material which results in increased losses in the hard magnetization direction. The ultra-flat core assembly results in a considerable stray flux in the winding window. Therefore, a reluctance model is presented which allows an accurate analytical calculation of the inductance value. Subsequently, **Section III** discusses the optimization of ultra-flat magnetic components with respect to minimum total footprint and/or minimum losses; the regarded design parameters are the core dimensions, the number of turns, the geometries of the windings, the maximum allowable losses per area, and the converter's specifications. The design of an ultra-flat flyback transformer, i.e. a two-winding inductor, is detailed. The design procedure can easily be adapted for ultra-flat inductors

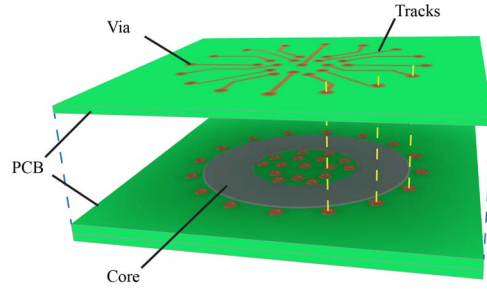


Fig. 2. PCB-integrated core; windings are realized with PCB tracks and vias.

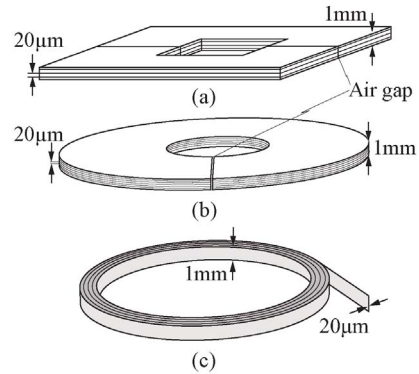


Fig. 3. Core configurations applicable to PCB-integrated transformers: (a) Two C-shaped core with stacked magnetic foils, (b) toroidal core with stacked magnetic foils including an air gap, and (c) toroidal core with a wound magnetic foil; in the last setup (c) an air gap can be manufactured with considerable effort.

as well. The results of the multi-objective optimization are presented as η - α -Pareto Front, which shows the trade-off between the area-related power density α (W/cm^2) and the efficiency η for a given magnetic core material. **Section IV** presents results obtained from a selected flyback-transformer design that are used to verify the theoretical considerations.

II. DESIGN CONSIDERATIONS FOR ULTRA-FLAT MAGNETIC COMPONENTS

A. Core geometry and core losses

In order to integrate an inductor or a transformer into a PCB, the setup of the core has to be taken into consideration. There are basically two types of constructions for PCB-integrated magnetics. The core can either be composed of a stack of thin magnetic foils (cf. Fig. 3(a) and (b)) or it consists of a thin toroidal wounded magnetic foil (cf. Fig. 3(c)). However, an air gap, which offers the designer an additional degree of freedom, can only be easily realized for stacked assemblies as toroidal wounded cores would fall apart. Only with a sophisticated attachment of the core inside of the PCB an air gap could be implemented.

An alternating magnetic flux in the core results in eddy current losses and hysteresis losses. A comparison between stacked and wounded cores, however, shows that equal eddy current losses result for both configurations; This is discussed in detail in the appendix of this paper.

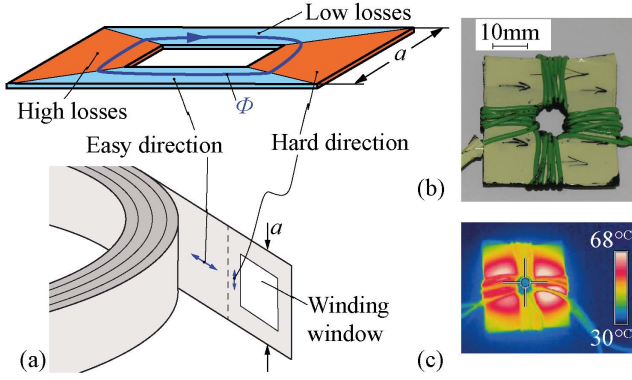


Fig. 4. (a) Magnetic sheets are cut out of a long band of magnetic foil. The flux will not only penetrate through the easy magnetizing direction but also through the hard direction. (b) A quadratic inductor consisting of 10 sheets (VC6155F by VAC [17]) is shown. The arrows indicate the easy direction. As can be seen in (c), the temperature rise in the hard direction is much higher compared to the easy direction (Measurement for $f_S = 100$ kHz, $\Delta B = 1.5$ T, $P_{\text{loss}} = 2.2$ W).

Hysteresis losses, however, show different behavior for both core constructions as there is an easy and a hard magnetizing direction in the foils. In toroidal wounded cores the flux is always in the tangential and therefore easy direction (cf. Fig. 4(a)). In magnetic cores consisting of a stack of magnetic foils, the flux will be forced to penetrate into the hard magnetizing direction as well. Fig. 4(a) shows that a foil is cut out of the magnetic band and a winding window is considered in the middle. The magnetic flux will flow as indicated in Fig. 4(a) and higher losses in the hard magnetization direction have to be expected.

Fig. 4(b) shows a quadratic prototype inductor which consists of a stack of ten VC6155F [17] foils (each $20 \mu\text{m}$ thick) with a length of 35 mm. Fig. 4(c) illustrates that a HF magnetic flux applied to the core results in different core losses for each direction; the temperature in the hard direction is higher compared to the easy direction. It is therefore crucial that the increased losses in the hard direction are considered in the design of a PCB-integrated inductor. Otherwise, the inductor could be thermally damaged due to the high losses in the hard direction. Thus, the Steinmetz parameters (k , α , and β) are extracted from measurements for the easy and the hard direction, which allow an accurate prediction of the core losses; Table II lists the extracted Steinmetz parameter of VC6155F and Metglas 2714A [18] for both directions.

In order to simplify the calculations for easy and hard directions a segmentation of the core as shown in Fig. 5 is assumed. The flux density in the core will decrease proportional to the inverse of the magnetic length $l_m(x)$. Thus, the maximum flux density B_{max} is at the inner border of the core (x_i or y_i). In the proposed design procedure either the saturation flux density or the losses limit the maximum flux density. Thus, the geometry of the core has to be designed in order to keep the maximum flux density within limits for a given flux.

Referring to Ampère's law and considering Fig. 5, the ratio of the flux density at the outer and the inner edge is

$$\frac{B(x = x_i)}{B(x = x_o)} = \frac{l_m(x = x_o)}{l_m(x = x_i)} = \frac{4 \cdot (x_o + y_o)}{4 \cdot (x_i + y_i)} \quad (1)$$

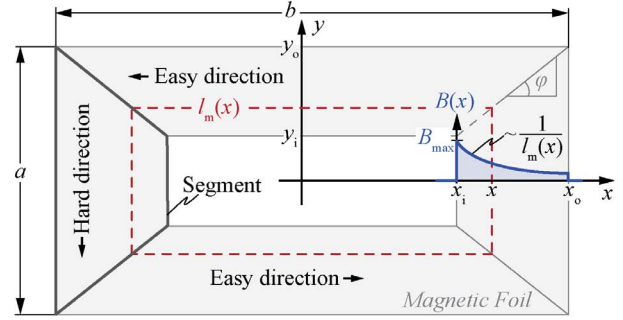


Fig. 5. Core geometry for the flux density calculation. The segments of easy and hard direction are indicated.

with

$$\begin{aligned} l_m(x) &= 4 \cdot (x + y_i + (x - x_i) \cdot \tan \varphi) \\ &= 4 \cdot \left(x + y_i + (x - x_i) \cdot \frac{y_o - y_i}{x_o - x_i} \right) \end{aligned}$$

The flux density at an arbitrary position x is thus

$$B(x) = B_{\text{max}} \cdot \frac{x_i + y_i}{x_i + y_i + (x - x_i) \cdot \frac{y_o - y_i}{x_o - x_i}} \quad (2)$$

and the core losses can be determined with the Steinmetz equation which has to be integrated over either an easy or a hard direction segment. For the hard direction the core losses are

$$P_v = 2 d_{\text{core}} k_{\text{fe}} \int_{x_i}^{x_o} \int_{-y_i - (x-x_i) \tan \varphi}^{y_i + (x-x_i) \tan \varphi} k \cdot f_S^\alpha \left(\frac{B(x)}{2} \right)^\beta dy dx, \quad (3)$$

with the core thickness d_{core} and the core fill factor k_{fe} . Equations similar to (2) and (3) can be determined for the easy magnetizing direction in the same way.

With these formulas the Steinmetz parameters of each direction can be extracted and the losses can be estimated in the magnetic design.

B. Materials

As already mentioned, nanocrystalline and amorphous materials are beneficial as ultra-thin bands of these materials are available. These bands feature a thickness of $20 \mu\text{m}$ or less and are applicable to HF applications. However, the width of the bands, a , (cf. Fig. 5 and Table II) is limited due to manufacturing reasons. This is a further limitation in the design process of an integrated inductor and causes the cores to be rather rectangular shaped than quadratic as otherwise the winding window ($4 \cdot x_i \cdot y_i$) would be too small to provide space to the windings.

Nanocrystalline materials are typically annealed in order to featuring the specified magnetic properties. However, after the annealing process these materials are very brittle, which makes a further mechanical treatment impossible. On the contrary, amorphous materials remain processable after being annealed.

Table II presents a comparison between the amorphous materials VC6155F [17] and 2714A [18], which are suitable for HF applications; it is shown that VC6155F has very low losses

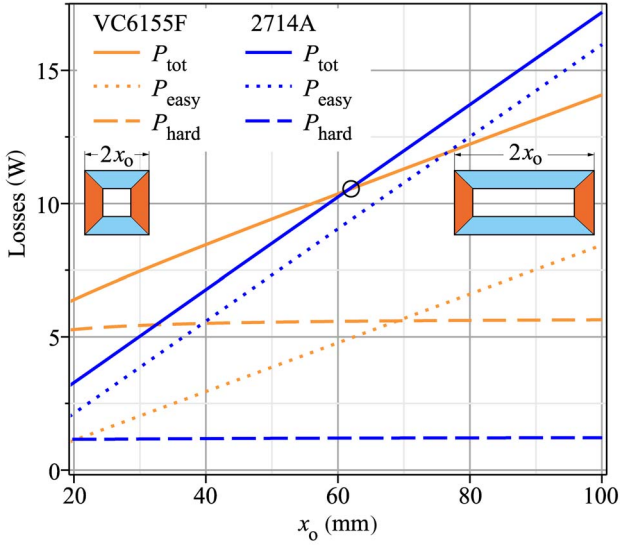


Fig. 6. Comparison between the losses in 2714A [18] and VC6155F [17]. As can be seen for rectangular cores with a large x_o , VC6155F exhibit lower losses whereas for quadratic cores 2714A is beneficial. The point where VC6155F becomes better is indicated in the figure (Parameters: $d_{\text{Core}} = 0.8$ mm, $x_i = x_o - 11.8$ mm, $y_i = 6.5$ mm, $y_o = 17.5$ mm, $f_s = 160$ kHz, $\Delta B = 0.8$ T).

in the easy direction but high losses in the hard direction. 2714A exhibits higher losses in the easy direction compared to VC6155F, however, lower losses in the hard direction.

For a quadratically shaped core, 2714A is thus beneficial as with VC6155F the losses in the hard direction would dominate the core losses. VC6155F is the material of choice if long core geometries are required as there 2714A suffers from high losses in the easy direction. Fig. 6 shows the losses in each direction for both materials whereas the length of the core x_o (cf. Fig. 5) is varied and the width of a rod ($x_o - x_i$) is kept constant. Fig. 6 points out that the losses in the hard direction keep constant while the losses in the easy direction increase due to the increased volume. Up to a core length of $x_o = 62$ mm 2714A would be the material of choice and above VC6155F features lower losses.

TABLE II
COMPARISON OF MAGNETIC MATERIALS FOR INTEGRATED CORES.

	Width a (mm)	B_{sat} (T)	Steinmetz parameters	
			Easy (W/m^3)	Hard (W/m^3)
VC6155F [17]	35	1.0	$k = 0.0043$ $\alpha = 1.84$ $\beta = 2.04$	$k = 0.074$ $\alpha = 1.71$ $\beta = 1.64$
2714A [18]	50	0.57	$k = 0.035$ $\alpha = 1.71$ $\beta = 1.91$	$k = 2.99$ $\alpha = 1.33$ $\beta = 2.24$

C. Core loss per area

For PCB-integrated magnetic components thermal issues are important as the generated heat has to be transferred through the PCB to the ambient. In order to keep the core temperatures within reasonable limits the maximum power loss per area p_{loss}

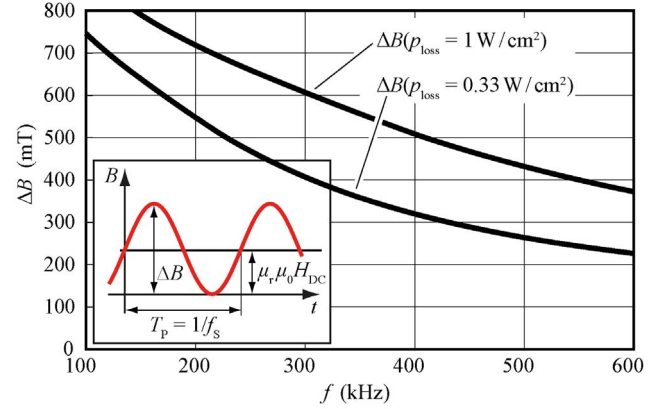


Fig. 7. Allowable ΔB for a specified power loss per area p_{loss} (Material: VC6155F, easy magnetizing direction). A dc offset H_{DC} which yields half of the peak-peak flux density has been considered.

has to be specified. Considering the Steinmetz equation

$$p_{\text{loss}} = k_{\text{fe}} \cdot d_{\text{Core}} \cdot k(H_{\text{DC}}) \cdot f_s^\alpha \cdot \left(\frac{\Delta B}{2}\right)^{\beta(H_{\text{DC}})} \quad (\text{W/m}^2) \quad (4)$$

the maximum allowable flux density swing ΔB can be determined in order to ensure the p_{loss} limitation. In (4) the impact of a dc offset H_{DC} can also be considered [19]. However, measurement results showed almost no impact of the dc offset for the considered materials (VC6155F and 2714A). Fig. 7 shows the calculation result for VC6155F in easy magnetizing direction; for a frequency of $f_s = 160$ kHz and a power loss per area $p_{\text{loss}} = 0.33$ W/cm² the flux density swing ΔB must not exceed 600 mT for a dc offset equivalent to 300 mT. In a design process the flux density is thus limited to the minimum of either ΔB or the saturation flux density B_{sat} .

D. Reluctance model

In an inductor or a transformer design process, the winding window has to allocate enough space for the windings. If the width of the magnetic band a is limited, the length of the core b (cf. Fig. 8(a)) has to be increased in order to provide enough space for all windings. Fig. 8(a) shows a typical setup where the windings are divided into n_w packages as this allows an interleaving with a secondary winding for transformer applications where a low leakage induction between the windings is crucial.

For $b \gg a$ the reluctance between the horizontal branches, the window reluctance $R_{m,\sigma}$, is not negligible. Furthermore, due to the ultra-flat core, the fringing of the flux in the air gap l_{air} and between the horizontal rods is vastly decreasing the reluctances $R_{m,\text{air}}$ and $R_{m,\sigma}$. An accurate analytical inductance calculation can only be achieved if the 3D fringing factors are considered. In [20] an analytical air gap calculation method including 3D fringing effects is presented, which is based on the Schwarz-Christoffel transformation. The consideration of these effects leads to an accurate reluctance model as illustrated in

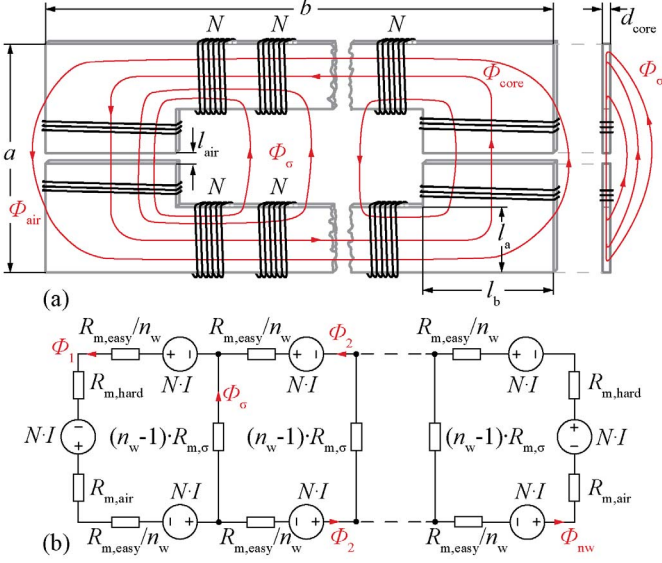


Fig. 8. (a) Setup of a PCB-integrated inductor; n_w winding packages, each with N turns, are placed around the core in order to facilitate an interleaving with a secondary winding. The reluctances $R_{m,\sigma}$ between the long magnetic rods have to be considered in the inductance calculation as they have considerable impact on the inductance for long cores lengths b . (b) Reluctance model of the setup presented in (a).

Fig. 8(b). The respective reluctances can be calculated with

$$R_{m,hard} = \frac{a - l_a}{\mu_0 \mu_r \cdot l_b d_{core} k_{fe}}, \quad R_{m,\sigma} = \frac{a - 2l_a - l_{air}}{\mu_0 \cdot (b - 2l_b) d_{core} k_{fe}} \cdot \sigma_s$$

$$R_{m,easy} = \frac{b - l_b}{\mu_0 \mu_r \cdot l_a d_{core} k_{fe}}, \quad R_{m,air} = \frac{l_{air}}{\mu_0 \cdot l_b d_{core} k_{fe}} \cdot \sigma_a, \quad (5)$$

whereas σ_s and σ_a are the 3D fringing factors [20] of the window reluctance $R_{m,\sigma}$ and the air gap reluctance $R_{m,air}$, respectively. The reluctance model in Fig. 8(b) can then be solved with standard electrical circuit analysis methods.

Table III presents the calculation and simulation results with and without considering fringing effects and window flux for the core geometry shown in Fig. 9(b). The conventional air gap calculation method would result in a large error. However, considering the fringing effects allows an accurate analytical calculation method for arbitrary core shapes. The results in Table III show that the impact of the $R_{m,\sigma}$ is small for this core setup which is also noticeable in the 3D simulation presented in Fig. 9(a). However, if the ratio between b and a (cf. Fig. 8(a)) increases, the window reluctance dominates the inductance calculation and a proper reluctance model is crucial.

TABLE III
INDUCTANCE CALCULATION COMPARISON (PARAMETERS: $a = 35$ mm, $b = 80$ mm, $l_A = 11$ mm, $l_B = 13$ mm, $l_{AIR} = 0.5$ mm, $d_{CORE} = 0.2$ mm, $N = 12$, $\mu_R = 1900$).

Calculation without window field and fringing	$L = 810$ nH
Calculation with fringing but without window field	$L = 3.58$ μ H
Calculation with fringing and window field	$L = 3.87$ μ H
3D simulation result	$L = 3.60$ μ H
Measurement result	$L = 3.83$ μ H

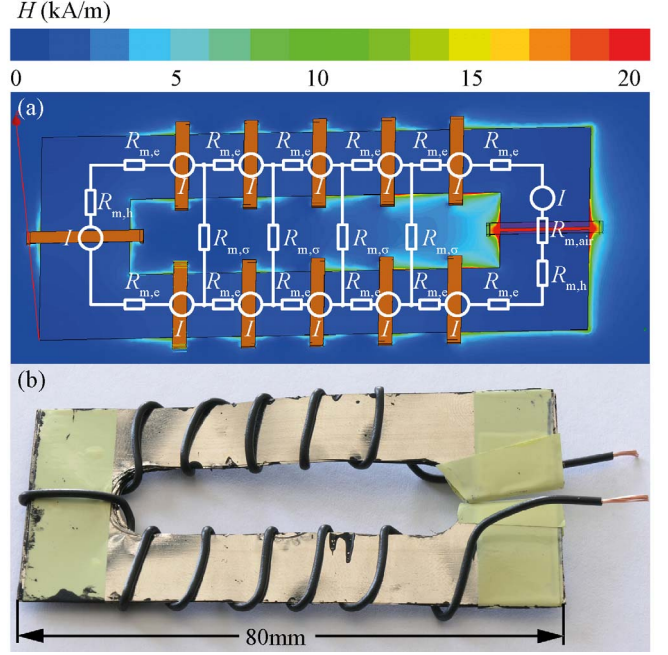


Fig. 9. (a) Reluctance model of an ultra-flat inductor and 3D simulation result of the magnetic field. The reluctances $R_{m,e}$ and $R_{m,\sigma}$ in the magnetic model are scaled with n_w and $(n_w - 1)$, respectively. The parameters are given in Table III together with the calculated and simulated inductance values. (b) Laboratory setup of the core consisting of ten stacked VC6155F foils.

III. TRANSFORMER DESIGN PROCEDURE

This section discusses the design and the optimization of a flyback transformer, i.e. a two-winding inductor, with a gapped rectangular core which is integrated into the PCB (cf. Fig. 3(a)). The presented multi-objective design procedure which is depicted in Fig. 10 can easily be adapted for an inductor or for different core configurations (e.g. toroidal cores, cf. Fig. 3(b) and (c)). Given all the input parameters shown in the block diagram, this step-by-step procedure leads to an optimal flyback transformer design.

In a first step the maximal allowable flux densities in the core, $B_{max,e}$ and $B_{max,h}$, are calculated for the easy and the hard magnetizing direction with respect to the maximum allowable power loss per area p_{loss} and the saturation flux density B_{sat} ; as indicated in Fig. 7, a dc offset in the flux density is considered in the loss calculation.

The next design step determines the geometries of the windings which is shown in Fig. 10(a); based on the maximum allowable current density J_{max} , the track width $b_{tr1,2}$, and the vias $d_{via1,2}$ (including the via pad annular ring d_{vp}) of primary and secondary windings can be calculated.

In order to keep the flux density within the evaluated limits, l_a and l_b (cf. Fig. 10(a)) have to be designed properly. An iterative procedure, depicted in Fig. 10, is implemented which starts with the calculation of an initial value of l_a that is neglecting the inhomogenous flux distribution in the core. With the required winding window length b_i , l_b can be calculated corresponding to (2). As now l_b and b_i are derived, l_a can be recalculated considering the inhomogenous flux distribution in the core which is followed by the next iteration step. The iteration stops as soon as $B_e < B_{max,e}$ and $B_h < B_{max,h}$.

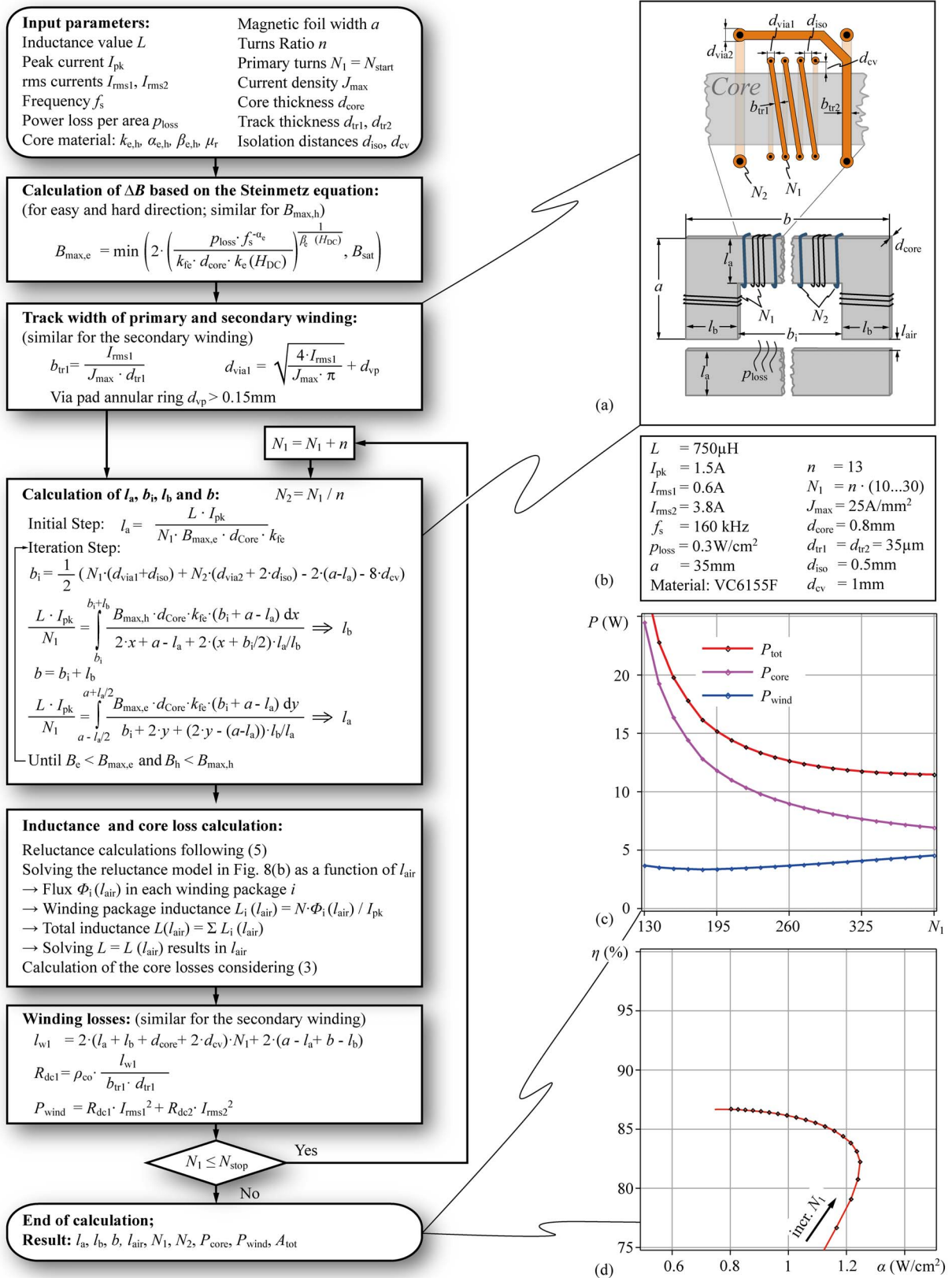


Fig. 10. Blockdiagram of the design procedure of a flyback transformer with PCB-integrated core. (a) Illustration of the flyback transformer which shows its dimensions. (b) Input parameter set. (c) Losses as a function of the number of turns for the parameters given in (b). (d) η - α -Pareto Front; a trade-off between the efficiency η and the area-related power density α has to be found for a given inductor or transformer.

The next step calculates the air gap length l_{air} by considering the reluctance model shown in Fig. 8(b). The core reluctances $R_{m,\text{easy}}$ and $R_{m,\text{hard}}$, the window reluctance $R_{m,\sigma}$, and the air gap reluctance $R_{m,\text{air}}$ are evaluated corresponding to (5). Solving the reluctance model as a function of l_{air} results in the flux $\Phi_i(l_{\text{air}})$ through each winding package i . The inductance $L_i(l_{\text{air}})$ of each series connected winding package i can be calculated as

$$L_i(l_{\text{air}}) = \frac{N \cdot \Phi_i(l_{\text{air}})}{I_{\text{pk}}}. \quad (6)$$

As the current I_{pk} is the same in each package i , the total inductance $L(l_{\text{air}})$ is the sum of all winding package inductances $L_i(l_{\text{air}})$. Then the air gap length l_{air} can be calculated by solving $L(l_{\text{air}}) = L$. The last step is the evaluation of the dc winding losses.

The design procedure is then iterated for a given number of turns $N = N_{\text{start}} \dots N_{\text{stop}}$. Fig. 10(c) shows the core losses P_{core} and the winding losses P_{wind} as a function of the turns N based on the parameters given in Fig. 10(b); minimal losses $P_{\text{tot}} = 11.5 \text{ W}$ are obtained for $N = 390$. Fig. 10(d) depicts a η - α -Pareto Front¹ and shows that a compromise between the efficiency η and the area-related power density α has to be found. The maximum power density for the considered design is $\alpha = 1.25 \text{ W/cm}^2$ and the maximum efficiency is $\eta = 86.7 \%$.

IV. EXPERIMENTAL RESULTS

In order to verify the presented design procedure a prototype of a flyback transformer for the PFC rectifier specified in Table I has been built up. Fig. 11(a) shows the transformer with the PCB-integrated core. For this prototype, the windings are realized with copper wires in order to be more flexible. Fig. 10(b) shows the design parameters and Table IV presents the resulting core geometries.

Although the core features an extreme aspect ratio the window reluctance $R_{m,\sigma}$ and the air gap reluctance $R_{m,\text{air}}$ are properly considered by the reluctance model; Fig. 11(b) presents the measurement of the magnetizing inductance which shows that the transformer has a slightly higher value of $L = 960 \mu\text{H}$ at 1 kHz (calculated: $750 \mu\text{H}$). At the switching frequency of $f = 160 \text{ kHz}$ the inductance decreases to $L = 870 \mu\text{H}$. The leakage inductance L_{σ} between primary and secondary windings of the transformer is $L_{\sigma} = 140 \mu\text{H}$ which is in good agreement with simulation results. Due to the high leakage inductance an active snubber [21] is considered in the flyback converter which recycles the energy in the leakage inductance; a circuit simulation has been used to verify the applicability of this transformer.

Fig. 11(c) illustrates the result of a saturation measurement; a current of $I_L = 1.5 \text{ A}$ can be applied to the flyback transformer without any saturation which has been specified in the design procedure.

¹ $\eta = P_{\text{out}} / (P_{\text{out}} + P_{\text{loss}})$, $\alpha = (P_{\text{out}} + P_{\text{loss}}) / (A_{\text{tot}})$, $A_{\text{tot}} \dots$ total required area

TABLE IV
PARAMETERS OF THE PROTOTYPE FLYBACK TRANSFORMER.

a	$= 35 \text{ mm}$	l_{air}	$= 10.3 \text{ mm}$
b	$= 171 \text{ mm}$	d_{Core}	$= 0.66 \text{ mm}$
l_a	$= 19 \text{ mm}$	N_1	$= 156$
l_b	$= 35.4 \text{ mm}$	N_2	$= 12$

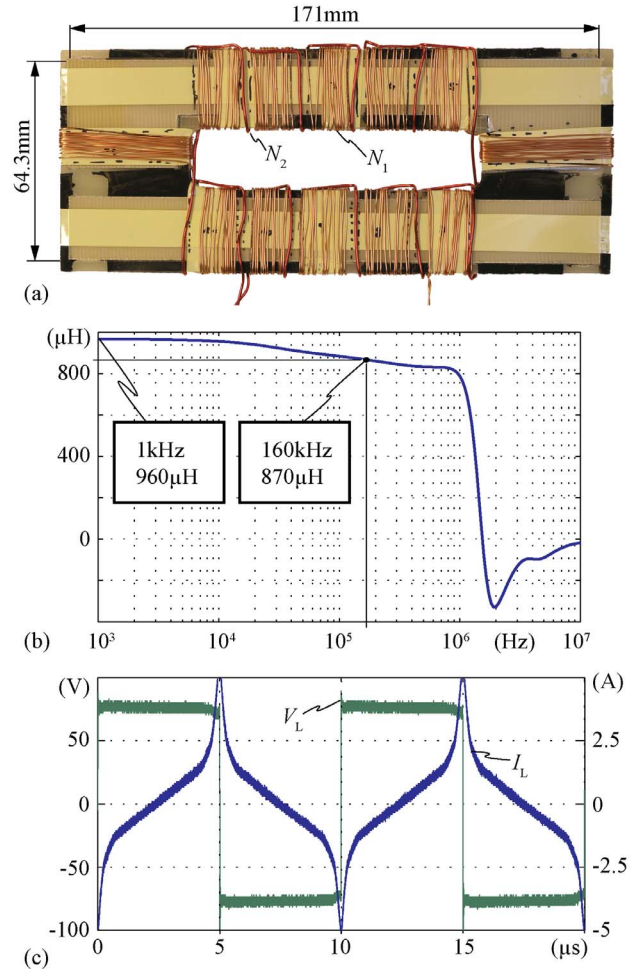


Fig. 11. (a) Prototype of a flyback transformer for a 35 W flyback-type PFC rectifier. The core thickness is $d_{\text{Core}} = 0.66 \text{ mm}$. (b) Magnetizing inductance L over the frequency of the prototype. (c) Saturation measurement results which confirms the specified saturation current of 1.5 A.

V. CONCLUSION

For the realization of a 1 mm thin PFC rectifier, the PCB-integration of magnetic components is a key issue. Therefore, this paper presents a multi-objective design procedure for ultra-flat magnetic components employing PCB-integrated cores. The proposed design procedure considers different electrical, magnetical, and geometrical parameters in order to determine the component's configuration that is optimal with respect to minimum losses and/or minimum footprint. The design procedure is applicable to inductors and transformers. Anisotropic core losses are considered and an accurate reluctance model is embedded in the design procedure which results in an accurate model of the PCB-integrated magnetic component. Measurement results verify the design procedure.

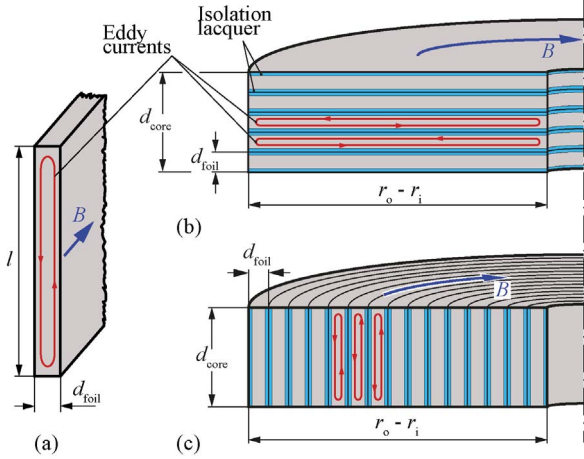


Fig. 12. (a) Eddy currents in a simple magnetic sheet. (b) Eddy currents in a core consisting of stacked magnetic foils; (c) eddy currents in a core setup with a toroidal wounded magnetic foil.

APPENDIX

EDDY CURRENT LOSSES IN STACKED AND TOROIDAL WOUNDED CORES

In this appendix it is shown that for both integrated core constructions (cf. Fig. 3(b) and (c)) the eddy current losses are equal. Consider a magnetic flux in a magnetic foil of a thickness d_{foil} and a width l (cf. Fig. 12(a)). Following Faraday's law

$$V = A_{\text{foil}} \cdot N \cdot \frac{dB}{dt} \propto A_{\text{foil}} = l \cdot d_{\text{foil}}, \quad (7)$$

a voltage will be induced in the magnetic material. This voltage will cause an eddy current as indicated in Fig. 12. The current depends on the resistance of the magnetic foil which is proportional to

$$R'_{\text{foil}} \propto \frac{l}{d_{\text{foil}}}, \quad (8)$$

whereas R'_{foil} is the resistance per unit length. Thus, the losses caused by these eddy currents are proportional to

$$P_{\text{loss}} \propto \frac{V^2}{R'} \propto \frac{l^2 \cdot d_{\text{foil}}^2}{l/d_{\text{foil}}} = l \cdot d_{\text{foil}}^3. \quad (9)$$

This expression gives a relation between the eddy current losses and the core geometry and will be applied to both cases of PCB-integrated inductors.

A. Core consisting of stacked magnetic foils

Considering Fig. 12(b), the number of stacked foils for a given core thickness d_{core} can easily be calculated with

$$N_{\text{foil}} = \frac{d_{\text{core}}}{d_{\text{foil}}}. \quad (10)$$

This can be substituted into (9) considering that the losses will now occur in N_{foil} sheets which results in

$$P_{\text{loss}} \propto \frac{d_{\text{core}}}{d_{\text{foil}}} \cdot l \cdot d_{\text{foil}}^3 = d_{\text{core}} \cdot d_{\text{foil}}^2 \cdot (r_o - r_i). \quad (11)$$

B. Core consisting of a wounded magnetic foil

For cores with a toroidal wounded magnetic foil (cf. Fig. 12(c)) the same procedure can be applied. In order to obtain the required inner and outer radii of the core (r_i and r_o , respectively), the number of windings N_{foils} is

$$N_{\text{foils}} = \frac{r_o - r_i}{d_{\text{foil}}}, \quad (12)$$

which can subsequently be substituted into (9):

$$P_{\text{loss}} \propto \frac{r_o - r_i}{d_{\text{foil}}} \cdot l \cdot d_{\text{foil}}^3 = (r_o - r_i) \cdot d_{\text{foil}}^2 \cdot d_{\text{core}}. \quad (13)$$

Comparing (11) and (13) it can be seen that the eddy current losses for both constructions are the same. This result has also been verified with 3D FEM simulations.

REFERENCES

- [1] D. Ge and Z. Chen, "On-chip boost DC-DC converter in color OLED driver & controller ICs for mobile application," in *6th International Conference on ASIC, ASICON*, vol. 1, pp. 459–463, 2005.
- [2] J. Jacobs, D. Hente, and E. Waffenschmidt, "Drivers for OLEDs," in *Conference Record of the 42nd IEEE Industry Applications Conference, IAS*, pp. 1147–1152, 2007.
- [3] J. Yoo, S. Jung, Y. Kim, S. Byun, J. Kim, N. Choi, S. Yoon, C. Kim, Y. Hwang, and I. Chung, "Highly flexible AM-OLED display with integrated gate driver using amorphous silicon TFT on ultrathin metal foil," *Journal of Display Technology*, vol. 6, no. 11, pp. 565–570, 2010.
- [4] S. Uchikoga, "Future trend of flat panel displays and comparison of its driving methods," in *IEEE International Symposium on Power Semiconductor Devices and IC's, ISPSD*, pp. 1–5, 2006.
- [5] I. Josifovic, J. Popovic-Gerber, and J. Ferreira, "A PCB system integration concept for power electronics," in *6th International IEEE Power Electronics and Motion Control Conference, IPEMC*, pp. 756–762, 2009.
- [6] C. Marxgut, J. Biela, and J. W. Kolar, "Design of a multi-cell, DCM PFC rectifier for a 1 mm thick, 200 W off-line power supply – The Power Sheet," in *Sixth International Conference on Integrated Power Electronic Systems, CIPS*, (Nuremberg), 2010.
- [7] "Infineon Technologies." <http://www.infineon.com>.
- [8] "Murata Manufacturing Co., Ltd." <http://www.murata.com>.
- [9] R. Ulrich and L. Schaper, "Putting passives in their place," *IEEE Spectrum*, vol. 40, no. 7, pp. 26–30, 2003.
- [10] "Vishay." <http://www.vishay.com>.
- [11] "EPCOS AG." <http://www.epcos.com>.
- [12] E. Waffenschmidt, B. Ackermann, and J. A. Ferreira, "Design method and material technologies for passives in printed circuit board embedded circuits," *IEEE Transactions on Power Electronics*, vol. 20, no. 3, pp. 576–584, 2005.
- [13] M. Ludwig, M. Duffy, T. O'Donnell, P. McCloskey, and S. Omathuna, "Design study for ultraflat PCB-integrated inductors for low-power conversion applications," *IEEE Transactions on Magnetics*, vol. 39, no. 5, pp. 3193–3195, 2003.
- [14] Q. Chen, Z. Gong, X. Yang, Z. Wang, and L. Zhang, "Design considerations for passive substrate with ferrite materials embedded in printed circuit board (PCB)," in *IEEE Power Electronics Specialists Conference, PESC*, pp. 1043–1047, 2007.
- [15] "Ferroxcube - ferrite cores, bobbins & accessories." <http://www.ferroxcube.eu>.
- [16] B. Bucheru, M. Davila, and I. Jitaru, "ZVS and ZCS high efficiency low profile adapter," in *Power Conversion Intelligent Motion Conference, PCIM, Shanghai, China, 2007*.
- [17] "Vacuumschmelze AG, VAC." <http://www.vacuumschmelze.de>.
- [18] "Metglas." <http://www.metglas.com>.
- [19] J. Muhlethaler, J. Biela, J. Kolar, and A. Ecklebe, "Core losses under DC bias condition based on steinmetz parameters," in *International Power Electronics Conference, (IPEC)*, pp. 2430–2437, 2010.
- [20] J. Muhlethaler, J. Kolar, and A. Ecklebe, "A novel approach for 3d air gap reluctance calculations," in *Eighth International Conference on Power Electronics, ICPE, ECCE Asia, 2011*.
- [21] G. Spiazzi, L. Rossetto, and P. Mattavelli, "Design optimization of soft-switched insulated DC/DC converters with active voltage clamp," in *Conference Record of the Thirty-First IEEE Industry Applications Conference, IAS*, vol. 2, pp. 1169–1176 vol.2, 1996.